Modulating Quantum Tunnelling of Magnetization in Dy isotopologue dimers

Ting-Ting Ruan,[a] Eufemio Moreno-Pineda,[b,c,d]* Sagar Paul,[d] Michael Schulze,[d] Sören Schlittenhardt,[a] Asato Mizuno,[e] Wolfgang Wernsdorfer,[d,*] and Mario Ruben[a,f,g,*]

[a]Institute of Nanotechnology (INT), Karlsruhe Institute of Technology (KIT), Hermann-von-Helmholtz-Platz 1, D-76344, Eggenstein-Leopoldshafen, Germany. E-mail: mario.ruben@kit.edu

[b]Universidad de Panamá, Facultad de Ciencias Naturales, Exactas y Tecnología, Depto. de Química-Física, Panamá, 0824, Panamá. E-mail: eufemio.moreno@up.ac.pa

[c]Universidad de Panamá, Facultad de Ciencias Naturales, Exactas y Tecnología, Grupo de Investigación de Materiales, Panamá, 0824, Panamá.

[d]Physikalisches Institut, Karlsruhe Institute of Technology (KIT), Engesserstraße 15, D-76131, Karlsruhe, Germany. E-mail: wolfgang.wernsdorfer@kit.edu

[e]Department of Life and Coordination-Complex Molecular Science, Institute for Molecular Science, 5-1 Higashiyama, Myodaiji, Okazaki, Aichi 444-8787, Japan

[f] Institute of Quantum Materials and Technologies (IQMT), Karlsruhe Institute of Technology (KIT), Hermann-von-Helmholtz-Platz 1, D-76344, Eggenstein-Leopoldshafen, Germany.

[g]Centre Européen de Sciences Quantiques (CESQ), Institutde Science et d'Ingénierie Supramoléculaires (ISIS), 8 allée Gaspard Monge, BP 70028, 67083, Strasbourg Cedex, France.

Science et d'Ingénierie Supramoléculaires (ISIS), 8 allée Gaspard Monge, BP 70028, 67083, Strasbourg Cedex, France.

1. Experimental Section

1.1. Reagents and Instruments

The ligand 3,6-Di-2-pyridyl-1,2,4,5-tetrazine was purchased from Aldrich. Precursor complexes [Dy(BTFA)$_3$(H$_2$O)$_2$] were synthesized following the reported procedures.[1,2] Elemental analysis data were obtained with a Vario MicroCube CHNS analyzer. Magnetic susceptibility measurements were measured using a Quantum Design MPMS-XL SQUID magnetometer on polycrystalline samples (12.3 mg for $1^{(I=5/2)}$ und 13.9 mg for $2^{(I=0)}$) in the temperature range of 2 to 300 K under a DC magnetic field (H_{DC}) of 1 kOe. The AC data was collected using an oscillating magnetic field of 3.5 Oe and frequencies between 1 Hz and 1.5 kHz. Diamagnetic contributions from the sample holder and eicosane were corrected for the DC data. Core diamagnetic corrections were performed employing Pascal's constants. Magnetization data was collected with a Quantum Design MPMS3 SQUID magnetometer equipped with a 7 T magnet. Low temperature (0.03 - 5 K) magnetization measurements were performed on single crystals using a μ-SQUID apparatus at different sweep rates between 0.128 and 0.005 T s^{-1}. The time resolution is approximately 1 ms. The magnetic field can be applied in any direction of the micro-SQUID plane with precision much better than 0.1° by separately driving three orthogonal coils. To ensure good thermalization, each sample was fixed with apiezon grease.

1.2. [(^{163}Dy(BTFA))$_2$(PHZP) $_2$] ($1^{(I=5/2)}$) and [(^{164}Dy(BTFA))$_2$(PHZP)$_2$] ($2^{(I=0)}$)

[^{163}Dy(BTFA)$_3$(H$_2$O)$_2$] (50 mg, 0.059 mmol) or [^{164}Dy(BTFA)$_3$(H$_2$O)$_2$] (50 mg, 0.059 mmol) were introduced into a solution containing 5 mL of ethanol and 1 mL of dichloromethane. Subsequently, the ligand 3,6-Di-2-pyridyl-1,2,4,5-tetrazine (bptz) (6.97 mg, 0.03 mmol) was added, and the mixture was stirred overnight at room temperature. After that slow evaporation at room temperature, resulting in the formation of block and orange crystals after a few days. Yield: 22.0 mg (46.02 %) for $1^{(I=5/2)}$, 27.3 mg (56.56 %) for $2^{(I=0)}$. Anal. Calcd. for [^{163}Dy$_2$(BTFA)$_4$(PHZP)$_2$] (1):

C, 46.91; H, 2.56; N, 6.84. Found: C, 46.67; H, 2.41; N, 6.73. Anal. Calcd. for [^{164}Dy$_2$(BTFA)$_4$(PHZP)$_2$] (2): C, 46.86; H, 2.56; N, 6.83. Found: C, 46.82; H, 2.53; N, 6.75.

1.3. Crystal structure determinations

Single-crystal X-ray diffraction data were collected using STOE IPDS2T diffractometer with graphite mono-chromated MoKα radiation (λ=0.71073 Å). Crystals were mounted on a loop using oil, and the X-ray diffraction data were collected under a nitrogen stream. The frame data were integrated and corrected for absorption with CrysAlisPro 1.171.40.67a.[4] The structures were solved using intrinsic phasing methods (SHELXT 2018/2)[5] and were refined with full-matrix least-squares procedures on F^2 using SHELXL 2018/3[5] implemented in Olex2 1.5.[6] All non-hydrogen atoms were refined anisotropically, and all hydrogen atoms were placed at calculated positions and refined using a riding model. Full crystallographic details can be found in CIF format: see the Cambridge Crystallographic Data Centre database (CCDC 2337590, 2337589)

1.4. Theoretical Calculations

For the Complete-active-space self-consistent field (CASSCF) calculations of complexes **1**$^{(I=5/2)}$ and **2**$^{(I=0)}$, we employed MOLCAS 8.2.[7-9] CASSCF-SO calculations were performed on a binuclear Dy^{III}-Y^{III} fragment, using the crystallographic coordinates obtained from the SCXRD structures with no further optimisations. Basis sets from the ANO-RCC library[10-12] were employed with VTZP quality for Dy, VDZP quality for the coordinated N and O atoms, and VDZ quality for all distant atoms , using the second-order DKH transformation.[12] The molecular orbitals (MOs) were optimized in state-averaged CASSCF calculations. For this, the active space was defined by the nine 4f electrons in the seven 4f orbitals of Dy^{III}. Three calculations were performed independently for each possible spin state, where 21 roots were included for S = 5/2, 224 roots for S = 3/2, and 490 roots for S = 1/2 (RASSCF routine). The wavefunctions obtained from these CASSCF calculations were posteriorly mixed by spin-orbit coupling, where all 21 of the S = 5/2 states, 128 of the S = 3/2 states, and 130 of the S = 1/2 states were included (RASSI routine[14]). The resulting spin-orbit wavefunctions were decomposed into their CF wavefunctions in the ^{6}H$_{15/2}$ basis, employing the SINGLE_ANISO[15, 16] routine, and the magnetic susceptibility was calculated.

1.5. Dipolar Matrix

Dipolar interactions between two S_{eff} = ½ states can be calculated employing the following equation:

$$H_{dip} = \frac{\mu_0 \mu_B^2}{4\pi r^3} - \left[\bar{\bar{g}}_{A(\alpha,\beta,\gamma)}\cdot\bar{\bar{g}}_{B((\alpha,\beta,\gamma))} - 3\left(\bar{\bar{g}}_{A(\alpha,\beta,\gamma)}\cdot\vec{R}\right)\cdot\left(\vec{R}^T\cdot\bar{\bar{g}}_{B(\alpha,\beta,\gamma)}\right)\right]$$

where μ_B is the Bohr magneton, μ_0 the vacuum permittivity, r is the Ln⋯Ln distance obtained from crystal structures. $\bar{\bar{g}}_{A/B}$ is the g-matrix of ion A and B, and $\vec{R}$ is the directional unit vector between the two ions, based on the CASSCF results. The angles of the rotation matrix are the Euler angles, obtained from the CASSCF results, using the Z-Y'-Z'' convention according to the following equations:

$$\bar{\bar{R}}_{Z(\alpha)} = \begin{pmatrix} \cos\alpha & -\sin\alpha & 0 \\ \sin\alpha & \cos\alpha & 0 \\ 0 & 0 & 1 \end{pmatrix}$$

$$\bar{\bar{R}}_{Y(\beta)} = \begin{pmatrix} \cos\beta & 0 & \sin\beta \\ 0 & 1 & 0 \\ -\sin\beta & 0 & \cos\beta \end{pmatrix}$$

$$\bar{\bar{R}}_Z = \begin{pmatrix} \cos\gamma & -\sin\gamma & 0 \\ \sin\gamma & \cos\gamma & 0 \end{pmatrix}$$

Table S1. Crystal Data and Structure Refinements for Complexes **1**$^{(l=5/2)}$ and **2**$^{(l=0)}$.

No.	1	2
Formula	$C_{64}H_{42}Dy_2F_{12}N_8O_{10}$	$C_{64}H_{42}Dy_2F_{12}N_8O_{10}$
Fw	1637.05	1639.05
T(K)	160	180
crystal system	triclinic	triclinic
space group	P-1	P-1
a , Å	13.5218(5)	13.5306(5)
b , Å	13.9480(7)	13.9571(6)
c , Å	18.7575(7)	18.7997(6)
α , deg	92.973(3)	92.968(3)
β , deg	100.359(3)	100.310(3)

For the calculation of the dipolar matrix, the reference frame was chosen to lie perpendicular to the Dy···Dy axis (y-axis).

Due to the highly axial ligand field parameters observed in the CASSCF-SO calculations, with highly axial *g*-factors the *g*-matrix for the Dy(III) in a $S_{eff}=\dfrac{1}{2}$ formalism is:

$$\bar{\bar{g}}_{Dy(1)} = \bar{\bar{g}}_{Dy(2)} = \begin{pmatrix} 0 & 0 & 0 \\ 0 & 0 & 0 \\ 0 & 0 & 20 \end{pmatrix}$$

These two ions are connected by a unit vector of the form:

$$\vec{R} = \begin{pmatrix} 0 \\ 1 \\ 0 \end{pmatrix}$$

Thus, this leads to a dipolar matrix for two Dy(III) ions separated by a distance of 4.064(3) Å and with $\alpha_{Dy(1)}$ = 122°, $\beta_{Dy(1)}$ = 158° and $\gamma_{Dy(1)}$ = 0° and $\alpha_{Dy(2)}$ = 134°, $\beta_{Dy(2)}$ = 9° and $\gamma_{Dy(2)}$ = 0°. The obtained dipolar matrix has the form (for an +*J* Hamiltonian):

$$J_{dip} = \begin{pmatrix} -0.054 & +0.056 & +0.488 \\ +0.086 & -0.089 & -0.782 \\ -0.251 & +0.260 & +2.282 \end{pmatrix} \text{cm}^{-1}$$

Which for a *J* = 15/2 is:

$$J_{dip} = \begin{pmatrix} -2.4\times10^{-4} & +2.5\times10^{-4} & +2.2\times10^{-3} \\ +3.8\times10^{-4} & -3.9\times10^{-4} & -3.5\times10^{-3} \\ -1.1\times10^{-3} & +1.2\times10^{-3} & +1.0\times10^{-2} \end{pmatrix} \text{cm}^{-1}$$

γ, *deg*	116.822(4)	116.870(4)
V (Å³)	3069.89(3)	3080.0(2)
Z	2	2
$\rho_{Calcd.}$ (mg·m⁻³)	1.77	1.764
μ (mm⁻¹)	2.519	2.511
R_{int}	0.072	0.050
GOF on F^2	0.978	1.031
R_1, wR_2 (I > 2σ(I))[a]	R_1 = 0.0434, wR_2 = 0.0917	R_1 = 0.0323, wR_2 = 0.752
R_1, wR_2(all data)	R_1 = 0.0680, wR_2 = 0.1022	R_1 = 0.427, wR_2 = 0.0796

[a] $R_1 = \sum||F_o| - |F_c||/\sum|F_o|$, $wR_2 = \{\sum w[(F_o)^2 - (F_c)^2]^2/\sum w[(F_o)^2]^2\}^{1/2}$

Table S2. Dy^{III} ion geometry analysis of **1**$^{(I=5/2)}$ and **2**$^{(I=0)}$ using the SHAPE 2.1

software.

	1$^{(I=5/2)}$		2$^{(I=0)}$	
	Dy1	**Dy2**	**Dy1**	**Dy2**
EP-9	33.930	32.429	33.894	32.449
OPY-9	22.997	23.174	23.008	23.262
HBPY-9	17.426	17.452	17.524	17.442
JTC-9	15.245	15.132	15.211	15.109
JCCU-9	8.679	8.564	8.696	8.543
CCU-9	7.795	7.718	7.794	7.716
JCSAPR-9	2.678	3.088	2.661	3.082
CSAPR-9	2.112	2.435	2.064	2.424
JTCTPR-9	2.041	2.340	2.020	2.340
TCTPR-9	**1.885**	2.648	**1.858**	2.641
JTDIC-9	11.277	10.550	11.268	10.575
HH-9	8.269	7.461	8.290	7.448
MFF-9	1.990	**2.253**	1.987	**2.250**

EP-9 = (D_{9h}) Enneagon
OPY-9 = (C_{8v}) Octagonal pyramid
HBPY-9 = (D_{7h}) Heptagonal bipyramid
JTC-9 = (C_{3v}) Johnson triangular cupola J3
JCCU-9 = (C_{4v}) Capped cube J8
CCU-9 = (C_{4v}) Spherical-relaxed capped cube
JCSAPR-9 = (C_{4v}) Capped square antiprism J10
CSAPR-9 = (C_{4v}) Spherical capped square antiprism
JTCTPR-9 = (D_{3h}) Tricapped trigonal prism J51
TCTPR-9 = (D_{3h}) Spherical tricapped trigonal prism
JTDIC-9 = (C_{3v}) Tridiminished icosahedron J63
HH-9 = (C_{2v}) Hula-hoop
MFF-9 = (C_s) Muffin
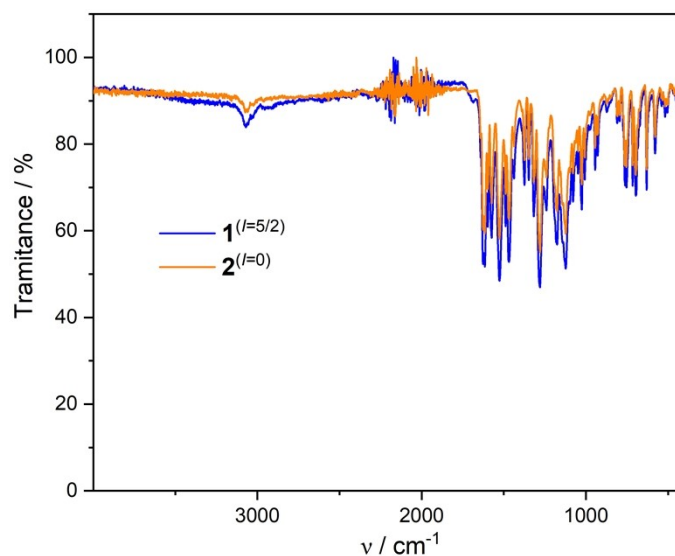
Figure S1. Infrared spectra for compound **1**$^{(I=5/2)}$ (blue) and **2**$^{(I=0)}$ (orange).
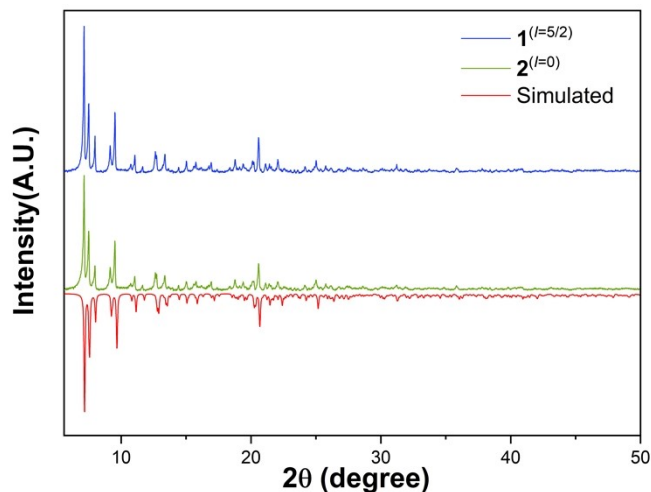
Figure S2. The room temperature simulated powder diffraction pattern (red) and experimental patterns for complexes $1^{(l=5/2)}$ (blue) and $2^{(l=0)}$ (green).
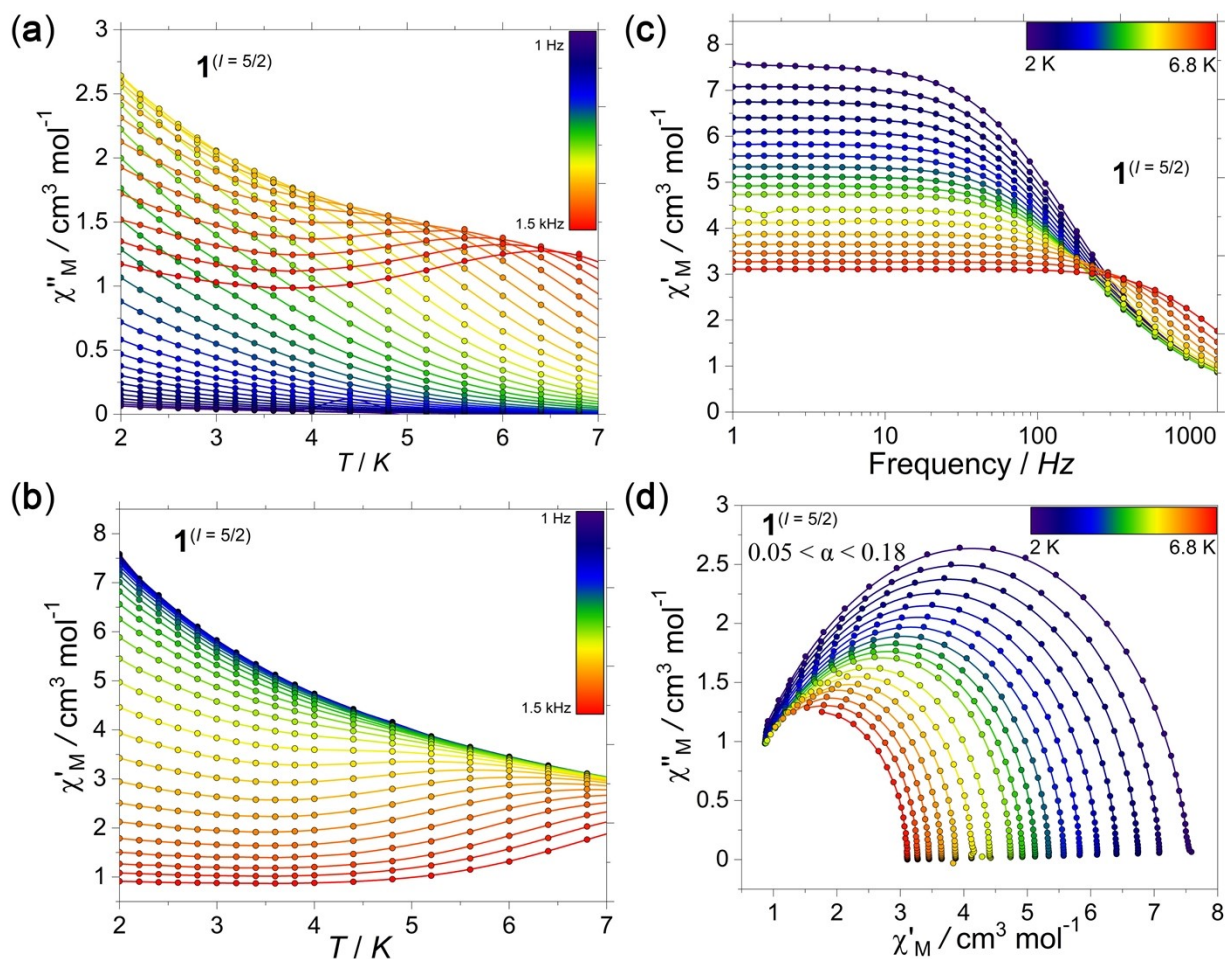
Figure S3. Dynamic magnetic data for $1^{(l=5/2)}$ employing a 3.5 Oe AC field and zero DC field. (a) $\chi_M''(T)$; (b) $\chi_M'(T)$; (c) $\chi_M'(\nu)$; (d) Cole-Cole plot.
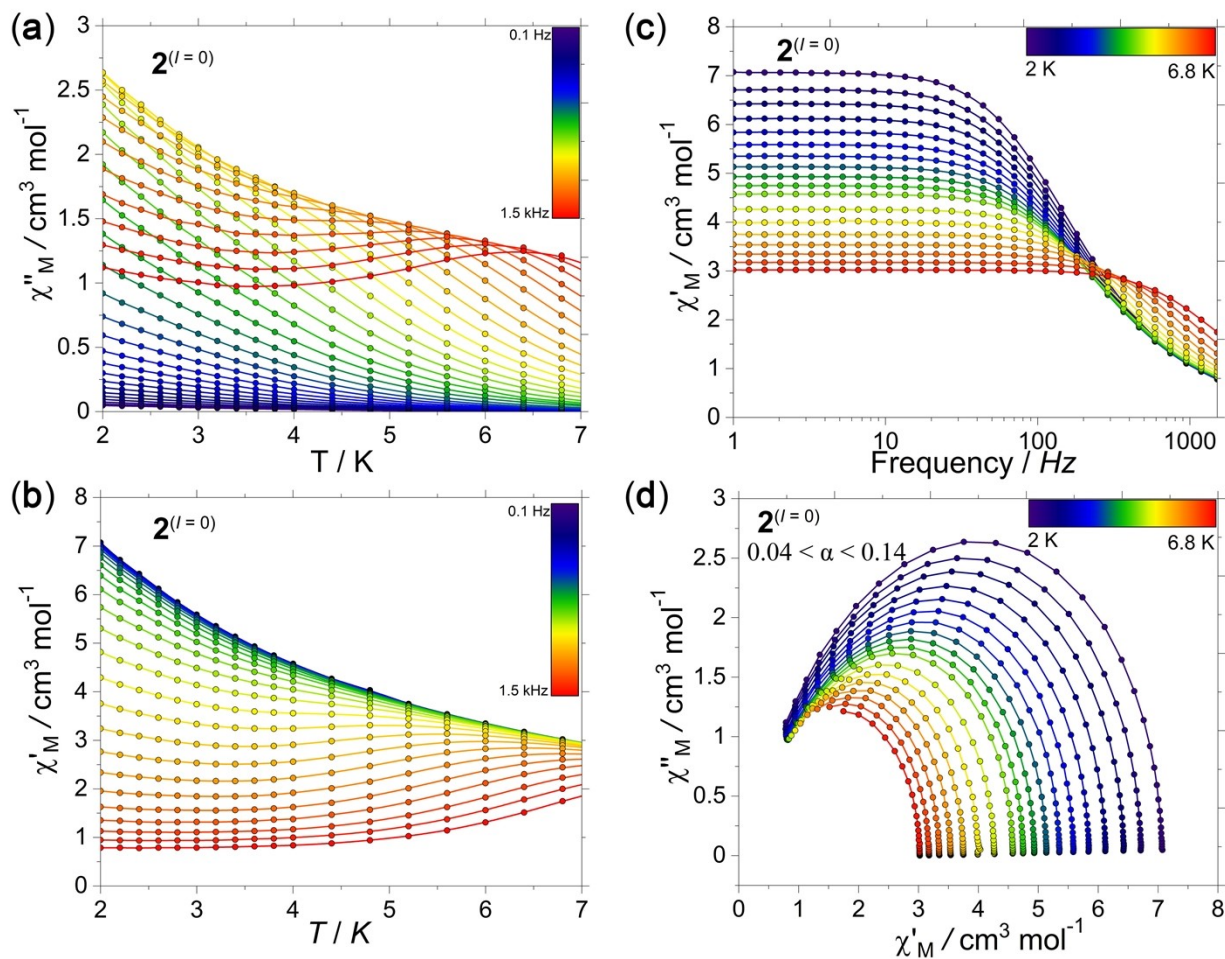
Figure S4. Dynamic magnetic data for **2**$^{(I=0)}$ employing a 3.5 Oe AC field and zero DC field. (a) $\chi_M''(T)$; (b) $\chi_M'(T)$; (c) $\chi_M'(v)$; (d) Cole-Cole plot.
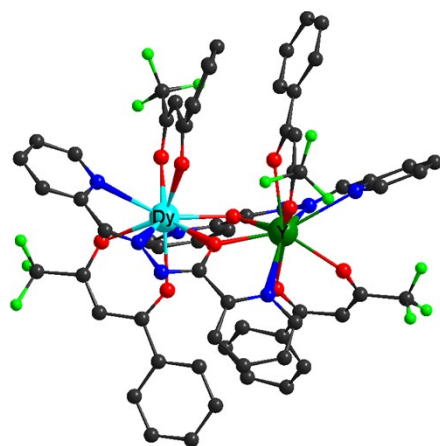
Figure S5. odel structures of individual Dy^{III} fragments of complexes **1−2**; H atoms are omitted for clarity.
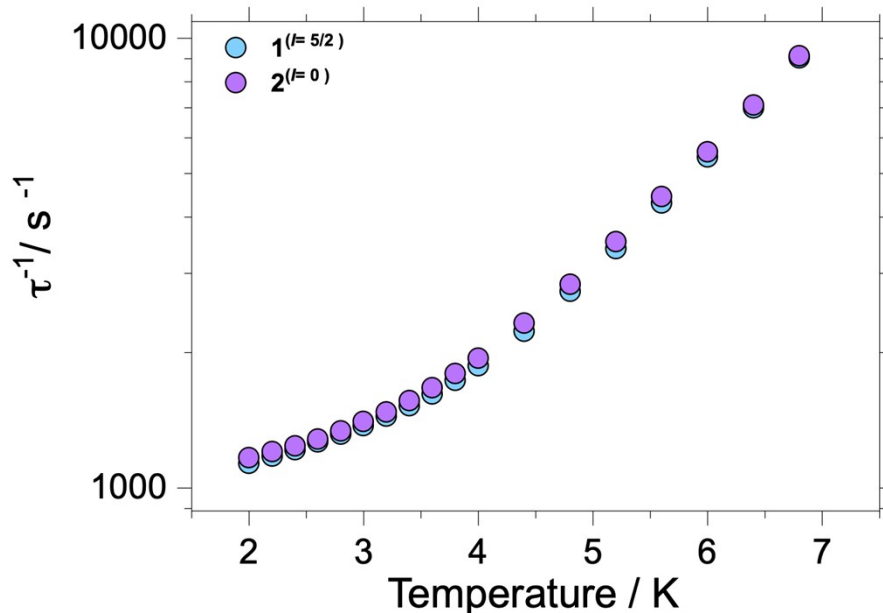
Figure S6. Experimental $\tau(T)$ for $\mathbf{1}^{(I=5/2)}$ (pale blue) and $\mathbf{2}^{(I=0)}$ (violet), exhibiting an almost superimposable behavior.
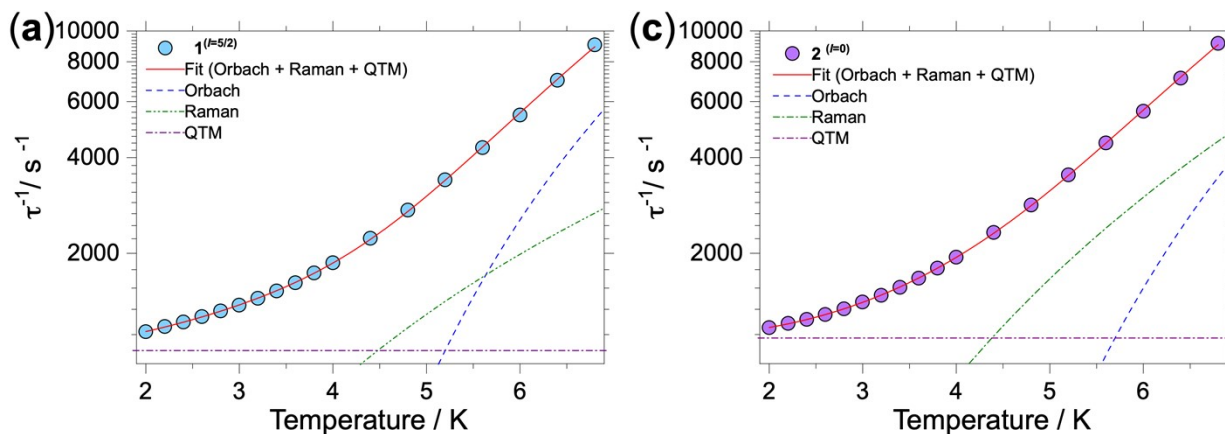
Figure S7. Experimental $\tau(T)$ for $\mathbf{1}^{(I=5/2)}$ (pale blue) and $\mathbf{2}^{(I=0)}$ (violet) and fits employing $\tau^{-1} = \tau_0^{-1} \exp(-U_{eff}/k_B T) + CT^n + \tau_{QTM}^{-1}$ (Orbach, Raman and QTM processes) (**a** and **b**) with the parameters given in the text. Note that the fits involving solely the Orbach and Raman processes yield low Raman n parameters.

Table S3. Electronic structure of individual $Dy^{III}(1)$ fragment calculated with CASSCF-SO using solid state geometry from $\mathbf{1}^{(I=5/2)}$.

Energy (cm⁻¹)	Energy(K)	g_x	g_y	g_z	Angle (°)
0.0	0.0	0.1270	0.2123	19.5920	
64.2	91.7	2.1567	3.3455	14.1170	82.8
87.9	125.6	9.7702	6.0402	1.2417	88.7
112.7	161.0	9.3013	6.0992	2.3640	44.6
165.8	236.9	0.9060	2.0077	13.8335	71.1
212.7	303.9	3.5360	4.8972	10.1428	57.9
245.8	351.2	3.2330	5.5899	11.7978	87.6
309.3	441.9	0.2439	0.4109	18.2398	89.9

Table S4. Electronic structure of individual $Dy^{III}(2)$ fragment calculated with CASSCF-SO using solid state geometry from $\mathbf{1}^{(I=5/2)}$.

Energy (cm^{-1})	Energy(K)	g_x	g_y	g_z	Angle (°)
0.0	0.0	0.1374	0.2240	19.5186	
77.9	111.3	1.9399	3.3141	14.6945	78.9
97.4	139.2	9.9252	6.8578	0.0420	70.9
134.2	191.7	2.2179	4.6029	10.0722	72.9
182.8	261.2	0.9230	3.4866	12.4208	86.0
220.7	315.3	0.4333	3.4735	12.2524	67.8
269.1	384.5	0.8007	3.5949	14.2039	74.7
300.4	429.2	0.5619	2.3228	16.6253	87.7

Table S5. Electronic structure of individual $Dy^{III}(1)$ fragment calculated with CASSCF-SO using solid state geometry from $\mathbf{2}^{(I=0)}$.

Energy (cm^{-1})	Energy(K)	g_x	g_y	g_z	Angle (°)
0.0	0.0	0.1059	0.1740	19.5772	
63.8	91.2	2.3158	4.0831	13.9450	79.2
90.2	128.9	0.7642	4.6922	9.1240	7.9
113.8	162.6	9.6585	6.9934	2.7444	37.1
165.3	236.2	0.8918	1.7038	14.0929	74.8
213.7	305.3	3.5333	5.5426	9.6008	60.6
245.9	351.3	3.1457	6.2442	11.2294	86.6
311.9	446.0	0.2284	0.3691	18.3112	89.1

Table S6. Electronic structure of individual $Dy^{III}(2)$ fragment calculated with CASSCF-SO using solid state geometry from $\mathbf{2}^{(I=0)}$.

Energy (cm^{-1})	Energy(K)	g_x	g_y	g_z	Angle (°)
0.0	0.0	0.1335	0.2358	19.5362	
85.2	121.7	2.0092	5.3978	12.3817	66.6
99.6	142.3	9.1636	5.7883	2.3075	53.7
137.8	196.9	2.2964	4.7120	9.8173	76.6
188.6	269.5	0.9496	3.0787	12.8107	82.1
227.8	325.5	0.1500	3.6551	12.3256	66.6
273.6	390.9	1.1684	3.6231	14.2851	76.8
307.0	438.6	0.5037	1.8134	16.8961	88.9

Table S7. Percentage composition of the lowest multiplet J = 15/2 for Dy1 in **1**$^{(l=5/2)}$.

m_J	Energy (K) of KD															
	0		91.7		125.6		161.0		236.9		303.9		351.2		441.9	
|-15/2>	0.0	97.1	0.5	0.0	0.0	0.1	1.0	0.0	0.0	0.6	0.0	0.5	0.1	0.0	0.0	0.0
|-13/2>	0.0	0.0	8.6	8.8	38.0	12.4	8.0	4.6	13.4	0.4	2.6	0.8	0.3	1.5	0.3	0.2
|-11/2>	0.0	1.5	5.7	2.6	4.1	1.3	17.7	6.6	10.5	8.8	0.0	35.8	0.7	3.3	0.3	0.8
|-9/2>	0.1	0.3	3.6	3.8	1.8	8.0	9.2	2.4	13.2	9.9	1.1	6.8	1.6	33.3	0.0	5.0
|-7/2>	0.0	0.4	0.9	4.7	3.8	3.9	20.4	1.4	12.5	1.5	7.1	5.8	16.7	2.3	18.4	0.0
|-5/2>	0.0	0.0	10.9	3.0	3.5	5.8	5.4	12.1	3.0	4.9	0.2	10.9	4.8	10.8	2.6	22.2
|-3/2>	0.0	0.5	9.5	7.8	11.1	4.4	1.8	5.0	0.5	10.9	0.1	1.4	14.1	8.8	13.5	10.6
|-1/2>	0.0	0.0	14.4	15.4	0.1	1.7	0.3	3.9	4.1	5.8	25.7	1.0	0.6	1.0	17.9	7.9
|+1/2>	0.0	0.0	15.4	14.4	1.7	0.1	3.9	0.3	5.8	4.1	1.0	25.7	1.0	0.6	7.9	17.9
|+3/2>	0.5	0.0	7.8	9.5	4.4	11.1	5.0	1.8	10.9	0.5	1.4	0.1	8.8	14.1	10.6	13.5
|+5/2>	0.0	0.0	3.0	10.9	5.8	3.5	12.1	5.4	4.9	3.0	10.9	0.2	10.8	4.8	22.2	2.6
|+7/2>	0.4	0.0	4.7	0.9	3.9	3.8	1.4	20.4	1.5	12.5	5.8	7.1	2.3	16.7	0.0	18.4
|+9/2>	0.3	0.1	3.8	3.6	8.0	1.8	2.4	9.2	9.9	13.2	6.8	1.1	33.3	1.6	5.0	0.0
|+11/2>	1.5	0.0	2.6	5.7	1.3	4.1	6.6	17.7	8.8	10.5	35.8	0.0	3.3	0.7	0.8	0.3
|+13/2>	0.0	0.0	8.8	8.6	12.4	38.0	4.6	8.0	0.4	13.4	0.8	2.6	1.5	0.3	0.2	0.3
|+15/2>	97.1	0.0	0.0	0.5	0.1	0.0	0.0	1.0	0.6	0.0	0.5	0.0	0.0	0.1	0.0	0.0

Table S8. Percentage composition of the lowest multiplet J = 15/2 for Dy2 in **1**$^{(l=5/2)}$.

m_J	Energy (K) of KD															
	0		111.3		139.2		191.7		261.2		315.3		384.5		429.2	
|-15/2>	0.0	95.6	0.0	0.6	0.3	0.0	1.6	0.0	0.0	0.8	0.5	0.3	0.0	0.1	0.0	0.0
|-13/2>	0.0	0.1	13.1	6.6	28.2	18.6	1.7	11.2	9.6	0.8	4.4	1.2	2.1	1.3	0.6	0.3
|-11/2>	0.0	2.4	2.5	8.6	3.5	1.2	15.5	10.4	7.8	6.1	10.5	16.8	4.0	6.6	2.3	1.8
|-9/2>	0.0	0.5	3.4	3.0	2.2	14.7	6.4	2.7	7.9	6.7	20.3	0.4	11.9	10.2	6.9	2.5
|-7/2>	0.0	0.7	4.5	0.2	5.0	1.5	23.2	1.9	6.1	11.5	8.6	1.5	15.6	3.0	0.6	16.2
|-5/2>	0.0	0.1	8.1	3.8	3.6	2.4	0.9	19.7	4.5	8.7	5.4	3.4	6.8	16.2	15.3	1.0
|-3/2>	0.0	0.3	5.0	11.0	7.3	6.9	0.1	3.9	1.4	17.8	3.8	3.3	8.5	6.6	13.4	10.7
|-1/2>	0.1	0.0	27.4	2.0	3.1	1.5	0.5	0.2	2.5	7.6	13.7	6.0	2.6	4.4	8.6	19.6
|+1/2>	0.0	0.1	2.0	27.4	1.5	3.1	0.2	0.5	7.6	2.5	6.0	13.7	4.4	2.6	19.6	8.7
|+3/2>	0.3	0.0	11.0	5.0	6.9	7.3	3.9	0.1	17.8	1.4	3.3	3.8	6.6	8.5	10.7	13.4
|+5/2>	0.1	0.0	3.8	8.1	2.4	3.6	19.7	0.9	8.7	4.5	3.4	5.4	16.2	6.8	1.0	15.3
|+7/2>	0.7	0.0	0.2	4.5	1.5	5.0	1.9	23.2	11.5	6.1	1.5	8.6	3.0	15.6	16.2	0.6
|+9/2>	0.5	0.0	3.1	3.4	14.7	2.2	2.7	6.4	6.7	7.9	0.4	20.3	10.2	11.9	2.5	6.9
|+11/2>	2.4	0.0	8.6	2.5	1.2	3.5	10.4	15.5	6.1	7.8	16.8	10.5	6.6	4.0	1.8	2.3
|+13/2>	0.1	0.0	6.6	13.1	18.6	28.2	11.2	1.7	0.8	9.6	1.2	4.4	1.3	2.1	0.3	0.6
|+15/2>	95.6	0.0	0.6	0.0	0.0	0.3	0.0	1.6	0.8	0.0	0.3	0.5	0.1	0.0	0.0	0.0

Table S9. Percentage composition of the lowest multiplet $J = 15/2$ for Dy1 in $\mathbf{2}^{(l=0)}$.

m_J	Energy (K) of KD															
	0		91.2		128.9		162.6		236.2		305.3		351.3		445.6	
|-15/2>	96.8	0.0	0.0	0.6	0.0	0.1	1.1	0.0	0.0	0.7	0.5	0.0	0.1	0.0	0.0	0.1
|-13/2>	0.0	0.0	9.1	11.5	46.4	4.8	8.4	1.6	11.9	1.0	0.5	2.3	1.1	0.8	0.3	0.2
|-11/2>	1.7	0.0	2.3	6.7	4.1	0.4	20.2	5.0	8.8	10.0	35.8	0.5	1.6	1.5	0.2	1.1
|-9/2>	0.4	0.1	4.0	4.0	4.2	5.1	8.5	3.1	11.5	11.0	5.3	0.8	17.2	19.6	0.2	5.1
|-7/2>	0.3	0.0	4.4	2.5	4.4	2.1	16.2	4.2	14.2	0.9	6.2	6.0	6.6	14.0	17.5	0.6
|-5/2>	0.1	0.0	1.2	11.2	1.1	8.1	7.4	10.6	3.1	5.6	12.5	0.1	12.0	2.5	3.3	21.4
|-3/2>	0.6	0.0	7.8	7.0	6.0	10.9	4.5	3.5	0.6	10.7	1.8	0.5	8.4	13.6	14.0	10.1
|-1/2>	0.0	0.0	9.2	18.6	1.4	1.0	0.1	5.5	4.8	5.3	1.6	25.5	0.4	0.6	17.7	8.2
|+1/2>	0.0	0.0	18.6	9.2	1.0	1.4	5.5	0.1	5.3	4.8	25.5	1.6	0.6	0.4	8.2	17.7
|+3/2>	0.0	0.6	7.0	7.8	10.9	6.0	3.5	4.5	10.7	0.6	0.5	1.8	13.6	8.4	10.1	14.0
|+5/2>	0.0	0.0	11.2	1.2	8.1	1.1	10.6	7.4	5.6	3.1	0.1	12.5	2.5	12.0	21.4	3.3
|+7/2>	0.0	0.3	2.5	4.4	2.1	4.4	4.2	16.2	0.9	14.2	6.0	6.2	14.0	6.6	0.6	17.5
|+9/2>	0.0	0.4	4.0	4.0	5.1	4.2	3.1	8.5	11.0	11.5	0.8	5.3	19.6	17.2	5.1	0.2
|+11/2>	0.0	1.7	6.7	2.3	0.4	4.1	5.0	20.2	10.0	8.8	0.5	35.8	1.5	1.6	1.1	0.2
|+13/2>	0.0	0.0	11.5	9.1	4.8	46.4	1.6	8.4	1.0	11.9	2.3	0.5	0.8	1.1	0.2	0.3
|+15/2>	0.0	96.8	0.6	0.0	0.1	0.0	0.0	1.1	0.7	0.0	0.0	0.5	0.0	0.1	0.1	0.0

Table S10. Percentage composition of the lowest multiplet $J = 15/2$ for Dy2 in $\mathbf{2}^{(l=0)}$.

m_J	Energy (K) of KD															
	0		121.7		142.3		196.9		269.5		325.5		390.9		438.6	
|-15/2>	0.0	95.8	0.0	0.5	0.0	0.4	0.0	1.7	0.0	0.7	0.0	0.7	0.1	0.0	0.0	0.0
|-13/2>	0.0	0.1	20.6	10.0	18.3	15.4	13.8	1.2	10.0	0.5	2.4	3.4	0.2	3.0	0.4	0.4
|-11/2>	0.0	2.4	3.3	8.2	1.1	3.8	5.9	20.4	7.6	7.1	3.1	22.9	1.7	8.6	1.4	2.4
|-9/2>	0.0	0.4	6.6	0.8	16.6	0.5	1.4	6.6	6.8	9.4	5.8	15.1	4.1	17.2	6.4	2.4
|-7/2>	0.0	0.7	2.3	0.2	2.8	6.8	2.2	23.2	8.2	7.4	3.9	6.3	9.4	10.7	2.6	13.0
|-5/2>	0.0	0.1	6.1	5.6	1.8	5.1	16.6	2.3	7.1	6.6	0.0	8.7	7.4	15.5	14.2	2.7
|-3/2>	0.0	0.2	4.2	7.6	6.4	11.2	4.2	0.1	0.1	19.1	0.8	5.8	1.6	14.1	13.0	11.8
|-1/2>	0.1	0.0	21.1	2.8	3.8	6.0	0.2	0.3	3.1	6.0	17.1	4.0	4.7	1.7	11.7	17.5
|+1/2>	0.0	0.1	2.8	21.1	5.9	3.8	0.3	0.2	6.0	3.1	4.0	17.1	1.7	4.7	17.5	11.7
|+3/2>	0.2	0.0	7.6	4.2	11.2	6.4	0.1	4.2	19.1	0.1	5.8	0.8	14.0	1.6	11.8	13.0
|+5/2>	0.1	0.0	5.6	6.1	5.1	1.8	2.3	16.6	6.6	7.1	8.7	0.0	15.5	7.4	2.7	14.2
|+7/2>	0.7	0.0	0.2	2.3	6.8	2.8	23.2	2.2	7.4	8.2	6.3	3.9	10.7	9.4	13.0	2.6
|+9/2>	0.4	0.0	0.8	6.6	0.5	16.6	6.6	1.4	9.4	6.8	15.1	5.8	17.2	4.1	2.4	6.4
|+11/2>	2.4	0.0	5.2	3.3	3.8	1.1	20.4	5.9	7.1	7.6	22.9	3.1	8.6	1.7	2.4	1.4
|+13/2>	0.1	0.0	10.0	20.6	15.4	18.3	1.2	13.8	0.5	10.0	3.4	2.4	3.1	0.2	0.4	0.4
|+15/2>	95.8	0.0	0.5	0.0	0.4	0.0	1.7	0.0	0.7	0.0	0.7	0.0	0.0	0.1	0.0	0.0

Table S11. Relaxation fitting parameters from the least-square fitting of the Cole-Cole plots of **1**$^{(I=5/2)}$ under a zero dc field at 2.0-6.8 K according to the generalized Debye model.

T / K	τ / s	χ_S / cm³mol⁻¹	χ_T / cm³mol⁻¹	α
2	8.98692E-4(8.70E-6)	0.43517(0.03151)	7.61995(0.01429)	0.18375(4.51E-3)
2.2	8.62321E-4(9.58E-6)	0.44507(0.03435)	7.16613(0.01527)	0.17783(5.22E-3)
2.4	8.35188E-4(9.67E-6)	0.44878(0.03430)	6.82692(0.01499)	0.17522(5.45E-3)
2.6	8.03373E-4(9.74E-6)	0.45021(0.03434)	6.484(0.01469)	0.17239(5.71E-3)
2.8	7.71238E-4(9.58E-6)	0.45147(0.03376)	6.17639(0.01412)	0.16998(5.85E-3)
3	7.39097E-4(9.46E-6)	0.45393(0.03350)	5.89617(0.01369)	0.16678(6.05E-3)
3.2	7.04485E-4(9.05E-6)	0.45822(0.03247)	5.63717(0.01292)	0.16253(6.09E-3)
3.4	6.67901E-4(8.71E-6)	0.45932(0.03196)	5.39703(0.01236)	0.15756(6.20E-3)
3.6	6.2811E-4(8.03E-6)	0.45468(0.03054)	5.17684(0.01141)	0.15203(6.10E-3)
3.8	5.85721E-4(7.38E-6)	0.45568(0.02942)	4.96901(0.01057)	0.14533(6.04E-3)
4	5.42833E-4(6.72E-6)	0.45559(0.02839)	4.77804(0.00977)	0.13804(5.96E-3)
4.4	4.54165E-4(6.69E-6)	0.44997(0.03006)	4.43382(0.01023)	0.12038(7.16E-3)
4.8	3.70155E-4(4.03E-6)	0.42808(0.02405)	4.15456(0.00649)	0.10853(5.21E-3)
5.2	2.95637E-4(2.86E-6)	0.42279(0.02116)	3.88487(0.00500)	0.08994(4.57E-3)
5.6	2.32404E-4(2.05E-6)	0.4059(0.01909)	3.66001(0.00359)	0.07624(3.94E-3)
6	1.8146E-4(1.56E-6)	0.40383(0.01821)	3.4574(0.00270)	0.06554(3.54E-3)
6.4	1.39812E-4(1.20E-6)	0.40058(0.01750)	3.27492(0.00194)	0.05587(3.11E-3)
6.8	1.07599E-4(1.07E-6)	0.41232(0.01935)	3.11249(0.00153)	0.05036(3.08E-3)

Table S12. Relaxation fitting parameters from the least-square fitting of the Cole-Cole plots of **2**$^{(I=0)}$ under a zero dc field at 2.0-6.8 K according to the generalized Debye model.

T / K	τ / s	χ_S / cm³mol⁻¹	χ_T / cm³mol⁻¹	α
2	8.6749E-4(1.08E-5)	0.43519(0.04007)	7.15145(0.01837)	0.14335(6.30E-3)
2.2	8.41902E-4(1.07E-5)	0.43764(0.03902)	6.79584(0.01759)	0.14282(6.42E-3)
2.4	8.17841E-4(1.05E-5)	0.43523(0.03803)	6.50417(0.01685)	0.14279(6.50E-3)
2.6	7.89937E-4(1.05E-5)	0.44129(0.03746)	6.19619(0.01627)	0.14241(6.68E-3)
2.8	7.57894E-4(1.02E-5)	0.44212(0.03630)	5.91277(0.01538)	0.1423(6.72E-3)
3	7.22316E-4(1.00E-5)	0.43677(0.03598)	5.65312(0.01481)	0.1419(6.88E-3)
3.2	6.88069E-4(9.33E-6)	0.44363(0.03405)	5.41204(0.01364)	0.13896(6.74E-3)
3.4	6.49415E-4(8.79E-6)	0.4472(0.03292)	5.18964(0.01275)	0.13605(6.72E-3)
3.6	6.08743E-4(8.16E-6)	0.44857(0.03183)	4.98367(0.01893)	0.13119(6.68E-3)
3.8	5.65169E-4(7.59E-6)	0.4455(0.03119)	4.79283(0.01114)	0.12731(6.67E-3)
4	5.22368E-4(6.71E-6)	0.44591(0.02931)	4.61427(0.01000)	0.12054(6.67E-3)
4.4	4.35333E-4(5.29E-6)	0.44089(0.02703)	4.29371(0.00824)	0.10763(6.40E-3)
4.8	3.56596E-4(3.91E-6)	0.43813(0.02394)	4.01977(0.00637)	0.09489(5.37E-3)
5.2	2.84617E-4(2.84E-6)	0.43073(0.02152)	3.76329(0.00484)	0.07965(4.76E-3)
5.6	2.24857E-4(2.08E-6)	0.41808(0.01959)	3.54568(0.00360)	0.06753(4.16E-3)
6	1.77118E-4(1.53E-6)	0.41947(0.01790)	3.35275(0.00261)	0.05667(3.59E-3)
6.4	1.37718E-4(1.17E-6)	0.42238(0.01691)	3.17883(0.00185)	0.04823(3.12E-3)
6.8	1.05976E-4(1.05E-6)	0.4294(0.01876)	3.0235(0.00146)	0.04264(3.09E-3)

Table S13. Crystal field Hamiltonian is given as $\hat{H}_{CF} = \sum\limits_{k,q} B_k^q O_k^q$ and the extended Stevens operator coefficients B_k^q are extracted from CASSCF calculations for **1**$^{(I=5/2)}$. (the calculation was performed for the individual centers).

		B_k^q	
k	q	Dy(1)	Dy(2)
2	-2	0.40594	0.07925
2	-1	0.12729	-0.10396
2	0	-0.96558	-0.97796
2	1	-0.39066	-0.37902
2	2	-0.34721	-0.34151
4	-4	-0.00139	0.00526
4	-3	-0.0314	-0.03563
4	-2	-0.0099	0.00292
4	-1	-0.00378	0.00295
4	0	-0.00262	-0.00287
4	1	0.01234	-0.00638
4	2	0.01038	0.01552
4	3	-0.02165	-0.00181
4	4	-0.00752	-0.00472
6	-6	-3.21596E-5	-4.01074E-4
6	-5	-2.72057E-4	-5.93512E-4
6	-4	6.93529E-5	-7.0557E-5
6	-3	2.27719E-4	2.98571E-4
6	-2	4.34607E-5	2.66551E-5
6	-1	7.16575E-5	-8.04648E-6
6	0	-1.70759E-6	-4.64531E-6
6	1	-1.64244E-4	1.6491E-4
6	2	-5.00765E-5	-7.66463E-5
6	3	1.49077E-4	-3.40594E-5
6	4	1.8932E-5	-5.81639E-5
6	5	-3.47508E-4	1.9475E-4
6	6	4.87906E-4	2.14491E-4

Table S14. Crystal field Hamiltonian is given as $\hat{H}_{CF} = \sum_{k,q} B_k^q O_k^q$ and the extended Stevens operator coefficients B_k^q are extracted from CASSCF calculations for $\mathbf{2}^{(l=0)}$. (the calculation was performed for the individual centers).

		B_k^q	
k	q	Dy(1)	Dy(2)
2	-2	0.41457	0.03988
2	-1	0.00267	-0.0053
2	0	-0.98126	-1.02135
2	1	-0.39068	-0.25712
2	2	-0.35867	-0.27121
4	-4	-0.00261	0.00473
4	-3	-0.03499	-0.03383
4	-2	-0.00969	0.00356
4	-1	-0.00256	0.00257
4	0	-0.00258	-0.00283
4	1	0.01229	-0.00725
4	2	0.00937	0.01595
4	3	-0.02124	8.82363E-4
4	4	-0.00783	-0.00522
6	-6	1.00507E-4	-3.58312E-4
6	-5	-5.03684E-4	-5.18833E-4
6	-4	5.81335E-5	-7.12983E-5
6	-3	2.54386E-4	2.82741E-4
6	-2	5.35494E-5	2.52442E-5
6	-1	7.7283E-5	-1.67247E-5
6	0	-9.05802E-7	-5.64632E-6
6	1	-1.57493E-4	1.62003E-4
6	2	-1.59175E-5	-8.58936E-5
6	3	1.56355E-4	-5.57658E-5
6	4	1.41521E-5	-5.35328E-5
6	5	-1.71664E-4	3.27554E-4
6	6	4.74592E-4	2.94064E-4

Table S15. Energy levels and state percentage composition for $\mathbf{1}^{(l=5/2)}$ and $\mathbf{2}^{(l=0)}$ employing the Lines model for the lowest three states.

State / Energy (K)	Ground	First	Second
$\mathbf{1}^{(l=5/2)}$	0	1.9	92
$\mathbf{2}^{(l=0)}$	0	1.4	94

(a) Dy1

Energy / cm^{-1} Energy / K Magnetic Moment / μ_B

0.18 x10^2
0.74
0.73
0.5 x 10^{-2}

(b) Dy2

Energy / cm^{-1} Energy / K Magnetic Moment / μ_B

0.16 x 10^2
1.1
0.49
0.6 x 10^{-2}

(c) Dy1

Energy / cm^{-1} Energy / K Magnetic Moment / μ_B

0.16 x 10^2
1.0
0.66
0.35 x 10^{-2}

(d) Dy2

Energy / cm^{-1} Energy / K Magnetic Moment / μ_B

0.14 x 10^2
1.6
0.71
0.65 x 10^{-2}
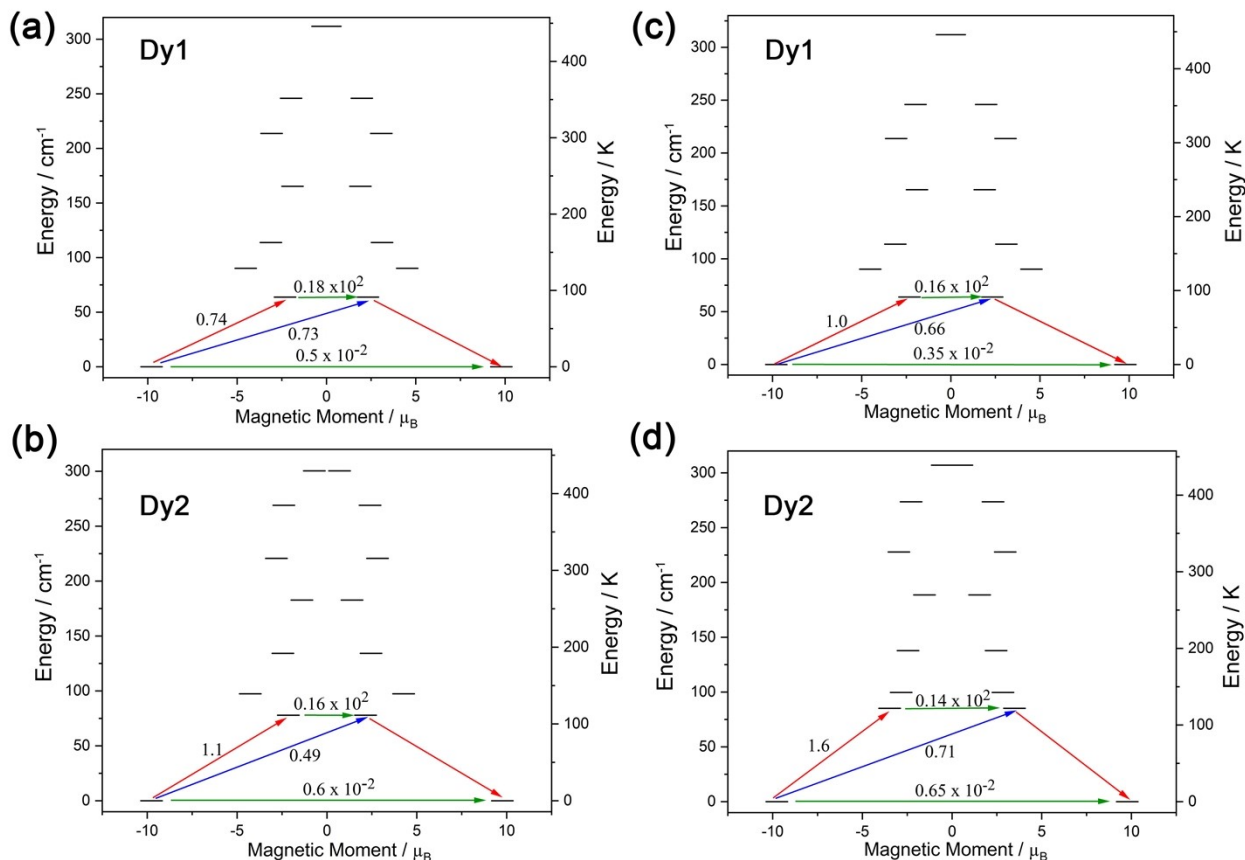
Figure S8. Magnetization blocking barriers for individual DyIII fragments in complexes **1** (left) and **2** (right). The thick black lines represent the KDs as a function of their magnetic moment along the magnetic axis. The green lines correspond to the diagonal matrix element of the transversal magnetic moment; the blue lines represent Orbach relaxation processes. The path shown by the red arrows represents the most probable path for magnetic relaxation in the corresponding compounds. The numbers at each arrow stand for the mean absolute value of the corresponding matrix element of the transition magnetic moment.

1.6. References

1. Yao, X.; Yan, P.; An, G.; Shi, C.; Li, Y.; Li, G., Single-ion magnets with D4d symmetry based on electron-donating β-diketonate Dy(iii) complexes. *New Journal of Chemistry* **2018,** *42* (11), 8438-8444.

2. Katagiri, S.; Tsukahara, Y.; Hasegawa, Y.; Wada, Y., Energy-Transfer Mechanism in Photoluminescent Terbium(III) Complexes Causing Their Temperature-Dependence. *Bulletin of the Chemical Society of Japan* **2007,** *80* (8), 1492-1503.

3. Brietzke, T.; Mickler, W.; Kelling, A.; Holdt, H. J., Mono- and dinuclear ruthenium(II) 1,6,7,12-tetraazaperylene complexes. *Dalton Trans* **2012,** *41* (9), 2788-97.

4. CrysAlisPro 1.171.39.46e, Rigaku Oxford Diffraction, 2018

5. Sheldrick, G. M., A short history of SHELX. *Acta Crystallogr A* **2008,** *64* (Pt 1), 112-22.

6. Dolomanov, O. V.; Bourhis, L. J.; Gildea, R. J.; Howard, J. A. K.; Puschmann, H., OLEX2: a complete structure solution, refinement and analysis program. *Journal of Applied Crystallography* **2009,** *42* (2), 339-341.

7. Aquilante, F.; Autschbach, J.; Carlson, R. K.; Chibotaru, L. F.; Delcey, M. G.; De Vico, L.; Fdez Galvan, I.; Ferre, N.; Frutos, L. M.; Gagliardi, L.; Garavelli, M.; Giussani, A.; Hoyer, C. E.; Li Manni, G.; Lischka, H.; Ma, D.; Malmqvist, P. A.; Muller, T.; Nenov, A.; Olivucci, M.; Pedersen, T. B.; Peng, D.; Plasser, F.; Pritchard, B.; Reiher, M.; Rivalta, I.; Schapiro, I.; Segarra-Marti, J.;

Stenrup, M.; Truhlar, D. G.; Ungur, L.; Valentini, A.; Vancoillie, S.; Veryazov, V.; Vysotskiy, V. P.; Weingart, O.; Zapata, F.; Lindh, R., Molcas 8: New capabilities for multiconfigurational quantum chemical calculations across the periodic table. *J Comput Chem* **2016,** *37* (5), 506-41.

8.   Ma, D.; Li Manni, G.; Gagliardi, L., The generalized active space concept in multiconfigurational self-consistent field methods. *J Chem Phys* **2011,** *135* (4), 044128.

9.   Siegbahn, P. E. M.; Almlöf, J.; Heiberg, A.; Roos, B. O., The complete active space SCF (CASSCF) method in a Newton–Raphson formulation with application to the HNO molecule. *The Journal of Chemical Physics* **1981,** *74* (4), 2384-2396.

10.   Roos, B. O.; Lindh, R.; Malmqvist, P. A.; Veryazov, V.; Widmark, P. O., Main group atoms and dimers studied with a new relativistic ANO basis set. *J Phys Chem A* **2004,** *108* (15), 2851-2858.

11.   Roos, B. O.; Lindh, R.; Malmqvist, P. A.; Veryazov, V.; Widmark, P. O.; Borin, A. C., New relativistic atomic natural orbital basis sets for lanthanide atoms with applications to the Ce diatom and LuF3. *J Phys Chem A* **2008,** *112* (45), 11431-5.

12.   Widmark, P., Malmqvist and BO Roos, T heor. Chim. P. *A. Acta* **1990,** *77*, 291.

13.   Peng, D.; Hirao, K., An arbitrary order Douglas-Kroll method with polynomial cost. *J Chem Phys* **2009,** *130* (4), 044102.

14.   AA, P., Malmqvist, BO Roos and B. Schimmelpfennig. *Chem. Phys. Lett* **2002,** *357*, 230.

15.   Chibotaru, L. F.; Ungur, L., Ab initio calculation of anisotropic magnetic properties of complexes. I. Unique definition of pseudospin Hamiltonians and their derivation. *J Chem Phys* **2012,** *137* (6), 064112.

16.   Ungur, L.; Chibotaru, L. F., Ab Initio Crystal Field for Lanthanides. *Chemistry* **2017,** *23* (15), 3708-3718.